J Therm Anal Calorim (2016) 123:1319–1327
DOI 10.1007/s10973-015-5094-y

# Smoke suppression and synergistic flame retardancy properties of zinc borate and diantimony trioxide in epoxy-based intumescent fire-retardant coating

**Feng Zhang[1] · Pengfei Chen[1] · Yong Wang[1] · Shaoxiang Li[1]**

Received: 25 February 2015 / Accepted: 10 October 2015 / Published online: 19 October 2015


**Abstract** In this article, smoke suppression and synergistic flame retardancy properties of zinc borate (ZB) and diantimony trioxide ($Sb_2O_3$) in epoxy-based intumescent fire-retardant (IFR) coating were investigated based on cone calorimeter test, smoke density test, scanning electron microscopy, thermogravimetric and Fourier transform infrared spectroscopic analyses. The measurement results of the dynamic combustion and smoke production behaviors and static smoke production behaviors of these IFR coatings showed that the values of heat release rate, smoke production rate, smoke factor and fire growth index all decreased significantly with the addition of ZB and $Sb_2O_3$. At the same time, the specific optical densities were remarkably reduced due to the existence of ZB and $Sb_2O_3$. These attractive data clearly demonstrated that the ZB and $Sb_2O_3$ had a good effect on smoke suppression and synergistic flame retardancy of the IFR coating. Besides, the scanning electron microscopy and the infrared spectroscopic analyses during coating thermal degradation were also carried out to explore the outstanding synergistic smoke suppression and flame retardancy mechanism of ZB and $Sb_2O_3$. With the melt of ZB and $Sb_2O_3$, a lot of heat was absorbed, and then, the glassy protective layer associated with the graphite char would effectively retard heat and suppress smoke.

**Keywords** Zinc borate · Diantimony trioxide · Intumescent fire-retardant coating · Smoke suppression · Heat release rate

✉ Feng Zhang
zhangfengqd@163.com

[1] College of Environment and Safety Engineering, Qingdao University of Science and Technology, 53 Zhengzhou Road, Qingdao 266042, People's Republic of China

## Introduction

Intumescent fire-retardant (IFR) coatings have been widely used to protect substrates against fire. At the same time, they are more environmentally friendly than the traditional halogen-containing flame-retardant coatings and have attracted considerable attention in recent years [1–5]. In addition, the IFR coatings can also present some outstanding advantages, for example, retaining the intrinsic properties of the material (e.g., the mechanical properties), easily processed and employed on multiple substrates (such as polymers, metallic materials, wood and textiles) [6–8].

The typical and widely studied IFR system is the combination of ammonium polyphosphate (APP), pentaerythritol (PER) and melamine (MEL) [9, 10]. Recently, many investigations demonstrate that expandable graphite (EG) has a high flame retardancy effect, no smoke production and low toxicity, which can expand in the perpendicular direction and generate a vermicular structured layer when exposed to a heat source. Accordingly, EG as a single component intumescent fire retardant has been widely used in the IFR composites. Moreover, the epoxy resin (EP) is still a superior material for IFR coatings as film former, due to its advantages, such as excellent chemical and corrosion resistance, high thermal and mechanical properties, low shrinkage upon cure, outstanding flexibility and electrical properties, and satisfactory adhesion to various substrates [11–15]. However, a serious problem in developing and applying EP is that a large amount of black smoke is produced when EP burns. So developing the epoxy-based IFR coating with good smoke suppression and flame retardancy properties is the key to further extend the IFR applications.

Many metal compounds, particularly transition metal compounds, have been reported to be effective smoke

suppression in epoxy-based IFR coating. There have been a great volume of literatures on the outstanding synergistic effects of zinc borate (ZB) and diantimony trioxide on smoke suppression and flame retardancy mechanism of halogen-containing flame-retardant coatings, which produce corrosive hydrogen halide and density smoke during combustion and do great harm to the environmental and public safety [16–18]. And yet, to the best of our knowledge, little previous work has been reported on the smoke suppression and flame retardancy of ZB and $Sb_2O_3$ for epoxy-based IFR coatings, which are widely regarded as one kind of outstanding halogen-free fire-retardant composites.

This paper mainly studies the smoke suppression and synergistic flame retardancy effect of ZB and $Sb_2O_3$ in epoxy-based IFR coating. The static and dynamic smoke production behaviors were investigated by smoke density test and cone calorimeter test, respectively. Furthermore, an intensive study on thermogravimetric and Fourier transform infrared spectroscopic analyses (TG-FTIR) during the coating degradation was carried out to reveal the smoke suppression mechanisms. Additionally, the residual char of the epoxy-based IFR coatings left after combustion was examined by scanning electron microscopy analysis.

## Experimental

### Materials

Commercial epoxy resin (E-44) was bought from Sinopec Baling Petrochemical Company, China. Polyamide resin (low molecular 650) used as curing agent was purchased from Zhenjiang Danbao resin Co., Ltd., China. Ammonium polyphosphate (G.R.) was obtained from Qingdao Haida Chemical Co., Ltd., China. Pentaerythritol (A.R.) was supplied by Tianjin Guangfu Chemical Co., Ltd., China. Melamine (A.R.) was a product from Shanghai Aibi Chemical Reagent Co., Ltd., China. Expandable graphite (EG) was produced by Qingdao Dongkai Graphite Co., Ltd., China. Zinc borate (A.R.) and diantimony trioxide (A.R.) were obtained from Qingdao Dayang Coating Factory, China. Dimethylbenzene (A.R.) was taken from Laiyang Economic and Technological Development Zone Fine Chemical Co., Ltd., China.

### Sample preparation

A certain amount of APP, PER, MEL, EG, $Sb_2O_3$ and ZB were mixed with EP which had dissolved in dimethylbenzene. Then the mixtures were ground into ultrafine particles by cone mill. After that, the PA dissolved in dimethylbenzene was added to the mixtures and stirred well. The end mixtures were then poured into specified size aluminum molds, and all the samples were dried for 2 weeks at ventilated place. The formulations of epoxy-based IFR coatings are listed in Table 1.

### Measurements

Fourier transform infrared (FTIR) spectrum was recorded between 500 and 4000 $cm^{-1}$ with an IR Prestige-21 spectrometer from Shimadzu Corporation, Japan.

The static smoke production behaviors of coating were measured by a smoke density test machine (JQMY-2, Jianqiao Co, China) according to ISO 5659.2-2006 and GB 8323.2-2008 with an incident flux of 25 or 50 kW $m^{-2}$. Each sample with dimension of 75 mm × 75 mm × 2 mm was put into an aluminum mold.

The cone calorimeter (Stanton Redcroft, UK) tests were performed according to ISO 5660 standard procedures with an external heat flux of 35 kW $m^{-2}$. Each sample with dimension of 100 mm × 100 mm × 2 mm was wrapped in an aluminum foil and then put into the specimen holder in the horizontal orientation for testing.

Thermogravimetric (TG) analyses were performed under nitrogen flow on a DT-50 (Setaram, France) instrument with crucible sample holders, at a heating rate of 20 K $min^{-1}$.

Scanning electron microscopy (SEM) studies were performed using a Hitachi X650 scanning electron microscope.

**Table 1** Formulations of the epoxy-based IFR coatings

| Sample code | APP/g | MEL/g | PER/g | EP/g | PA/g | EG/g | $Sb_2O_3$/g | ZB/g |
|---|---|---|---|---|---|---|---|---|
| IFR-0 | 30 | 12 | 18 | 36 | 24 | 0 | 0 | 0 |
| IFR-1 | 30 | 12 | 18 | 36 | 24 | 5 | 0 | 0 |
| IFR-2 | 30 | 12 | 18 | 36 | 24 | 5 | 5 | 5 |
| IFR-3 | 30 | 12 | 18 | 36 | 24 | 5 | 0 | 5 |
| IFR-4 | 30 | 12 | 18 | 36 | 24 | 5 | 5 | 0 |

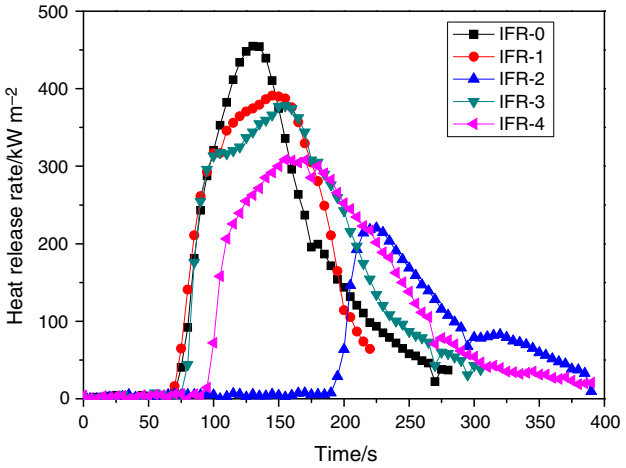


**Fig. 1** Heat release rate curves of the epoxy-based IFR coatings at a flux of 35 kW $m^{-2}$

## Results and discussion

### Cone calorimeter test

To obtain comprehensive understanding about dynamic combustion and smoke production behaviors of epoxy-based IFR coatings, the cone calorimeter test (CCT) was carried out and the typical parameters are illustrated in detail as follows.

Figure 1 shows the heat release rate (HRR) curves of all epoxy-based IFR coatings in the CCT. It can be seen that the IFR-0, IFR-1 and IFR-3 coatings ignited within 75 s after the test started. A sharp peak heat release rate (PHRR) of 454.9 kW $m^{-2}$ appeared rapidly for the IFR-0 coating after ignition. However, the PHRR values of the IFR-1 (391 kW $m^{-2}$) and IFR-3 (377.9 kW $m^{-2}$) coatings are lower, and the time to PHRR of these two coatings is about 25 s later than those of the IFR-0 coating.

The lower PHRR values of the IFR-1 and IFR-3 coatings indicate that the EG and ZB help to improve the flame retardancy performance of the epoxy-based IFR coatings. More specifically, the EG can promote the formation of char residue layer on the surface of the sample to prevent the burning of combustible materials derived from the degradation and the entrance of oxygen [19]. Furthermore, the HRR values of the IFR-3 coating are a little lower than those of the IFR-0 coating from 105 to 155 s, indicating that the ZB melts at high temperature to form glassy layer, which acts as a barrier to prevent heat from destroying the underlying materials [20].

$$2H_2BO_3 \xrightarrow{130-200\,^{\circ}C(-H_2O)} 2HBO_2 \xrightarrow{260-270\,^{\circ}C(-H_2O)}$$

$$B_2O_3 \xrightarrow{350\,^{\circ}C} \text{softening} \xrightarrow{500\,^{\circ}C} \text{porous material}$$

Compared with the IFR-3 coating, the IFR-4 coating shows a better performance on combustion behavior. With the addition of $Sb_2O_3$, the PHRR value decreases greatly (220.5 kW $m^{-2}$), and the time to ignition and PHRR is put off significantly. All these results indicate that the $Sb_2O_3$ has much better flame retardancy effects than the ZB; when the $Sb_2O_3$ was melting, a lot of heat could be absorbed, and then with the formation of a molten protective layer, the combustible materials were isolated and the underlying materials were protected effectively [21].

Attractively, the IFR-2 coating shows the lowest PHRR value and the longest time to ignition among all samples, indicating that the synergistic effect of ZB and $Sb_2O_3$ can effectively retard heat release during the whole combustion process. Therefore, both ZB and $Sb_2O_3$ can retard the sample to burn by condensed phase mechanism, displaying an excellent synergism when they are used together.

Figure 2 presents the total heat release (THR) of the epoxy-based IFR coatings. As the results showed, the THR values of the IFR-2 coating are greatly lower than those of other coatings throughout the entire combustion process.

It is reported that the gradient of THR curve can be assumed as representative of flame spread [22, 23]. Compared with the IFR-0, IFR-1 and IFR-3 coatings, the gradient of THR curve for the IFR-4 coating is greatly reduced, suggesting that the flame spread speed slows down. Specifically, in the case of the coating containing ZB and $Sb_2O_3$, the flame spread speed further decreases. All these results suggest that the synergism of ZB and $Sb_2O_3$ can not only improve the char residue to be more compact, but also help to restrict flame spread.

In most cases of real fire hazards, the major factor leading to death is the toxic substances and smoke released from the burning materials [24]; therefore, it is important to

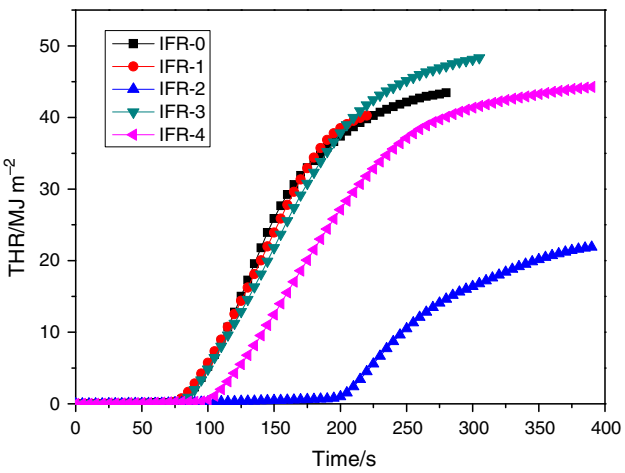


**Fig. 2** Total heat release curves of the epoxy-based IFR coatings at a flux of 35 kW $m^{-2}$

evaluate the smoke production behaviors of fire-retardant coatings. The smoke production rate (SPR) curves of the epoxy-based IFR coatings are illustrated in Fig. 3.

It can be seen that the peak smoke production rate (PSPR) value of the IFR-0 coating is 0.063 $m^2$ $s^{-1}$ at 101 s, while the PSPR value of the IFR-1 coating is 0.054 $m^2$ $s^{-1}$ at 120 s and the PSPR value of the IFR-3 coating is 0.046 $m^2$ $s^{-1}$ at 141 s. Hence, compared with the IFR-0 coating, the IFR-1 and IFR-3 coatings have lower PSPR values and longer time to PSPR. With regard to the IFR-2 containing both ZB and $Sb_2O_3$, the PSPR value (0.042 $m^2$ $s^{-1}$) is the lowest and the time to PSPR (127 s) is the longest.

Note that the time to PSPR of the IFR-4 coating (80 s) is the shortest, though it has a lower PSPR value (0.044 $m^2$ $s^{-1}$) than both the IFR-0 and IFR-1 coatings. The reason is that, although the melting $Sb_2O_3$ can absorb lots of heat and improve the char layer to suppress smoke, it tends to react with phosphate, derived from the degradation of APP, to form antimony phosphate that has a negative effect on smoke suppression in the early combustion stage. So an "antagonistic effect" will appear during the combustion process, which accelerates the decomposition of APP to form some smoke particles [25].

$$\mathrm{APP} \xrightarrow{\text{low temperature}} \mathrm{H_3PO_4} + \text{smoke precursors}$$

$$2\mathrm{H_3PO_4} + \mathrm{Sb_2O_3}(s) \rightarrow 2\mathrm{SbPO_4}(s) + 3\mathrm{H_2O}$$

With the addition of ZB, the phosphate will be neutralized effectively and the ZB will help to promote the formation of char layer so that the SPR values may decrease in the charring process. As a result, the smoke-forming and combustible materials substantially reduce in the gas phase. Based on the above discussion, it is reasonable to conclude that ZB and $Sb_2O_3$ are effective additives to suppress smoke during the whole combustion process.

Smoke factor (SF) is the product of PHRR and total smoke rate (TSR). It is an important parameter that represents a ratio of exhaust opacity to the amount of fuel burned at the time of measurement [26]. It can be calculated using Eq. (1):

$$\mathrm{SF} = \mathrm{PHRR} \times \mathrm{TSR} \tag{1}$$

From Fig. 4, it can be seen that the SF value for the IFR-0 coating is up to 239.4 MW $m^{-2}$, while the SF values for the IFR-1, IFR-2, IFR-3 and IFR-4 coatings are 192.5, 158.9, 204.2 and 174.3 MW $m^{-2}$, respectively, which are much lower than that of the IFR-0 coating. Moreover, compared with other coatings, the IFR-2 coating containing ZB and $Sb_2O_3$ shows the lowest SF values during the whole combustion process. Attractively, the SF values of the IFR-4 coating are higher than those of the IFR-3 coating within 100 s after the test began, indicating that the $Sb_2O_3$ has a negative effect on smoke suppression in the early combustion stage.

In order to explore the fire hazard comprehensively, the fire performance index (FPI) and the fire growth index (FGI) are calculated according to Eqs. (2) and (3) using cone calorimeter test data.

$$\mathrm{FPI} = \frac{t_{\mathrm{ig}}}{\mathrm{PHRR}} \tag{2}$$

$$\mathrm{FGI} = \frac{\mathrm{PHRR}}{t_{\mathrm{p}}} \tag{3}$$

The FPI (s $m^2$ $kW^{-1}$) is defined as the ratio of time to ignition (TTI or $t_{ig}$) and PHRR. There is a certain correlation between the FPI value and the time to flashover of material; the lower the FPI value is, the less time it will

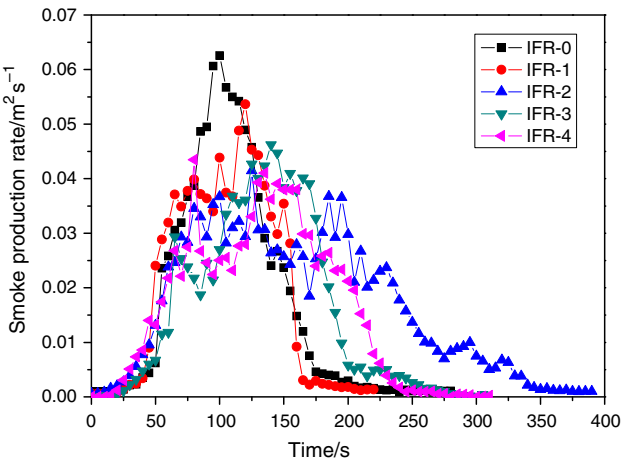


**Fig. 3** Smoke production rate curves of the epoxy-based IFR coatings at a flux of 35 kW $m^{-2}$

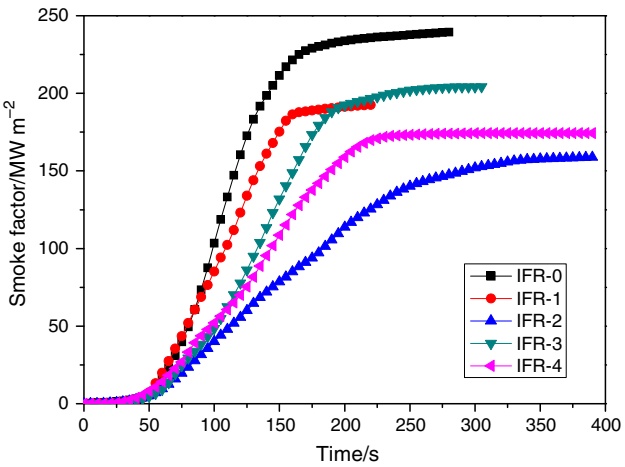


**Fig. 4** Smoke factor curves of the epoxy-based IFR coatings at a flux of 35 kW $m^{-2}$

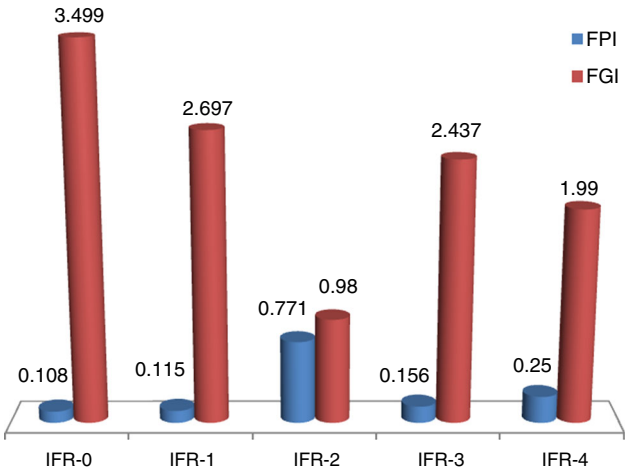


**Fig. 5** FPI and FGI for the epoxy-based IFR coatings at a flux of 35 kW $m^{-2}$

spend catching flashover and the higher the fire risk will be. The FGI (kW $m^{-2}$ $s^{-1}$) is defined as the ratio of PHRR and time to PHRR (TTP or $t_p$). The FGI reflects the fire development speed, and a higher FGI value means that the time to PHRR is shorter so that the fire risk is higher [27, 28]. Overall, materials with higher safety rank require high FPI values and low FGI values. From Fig. 5, it can be seen that the IFR-2 coating owns the highest FPI value and the lowest FGI value which indicates that it gets highest safety rank than other IFR coatings.

## Smoke density test

To get more information about the smoke performance of the epoxy-based IFR coatings, the static smoke production behavior tests for the IFR-0, IFR-1 and IFR-2 coatings were carried out under different incident heat fluxes and combustion conditions. Here, static smoke production behaviors were measured by the smoke density test. The specific optical density ($D_s$) curves of the epoxy-based IFR coatings are illustrated in Figs. 6 and 7.

It can be seen from Fig. 6a, the $D_s$ values of the IFR-1 coating containing only EG are lower than those of the IFR-0 coating under a radiant heat flux of 25 kW $m^{-2}$ without flame. When the ZB and $Sb_2O_3$ are added into the coating, the $D_s$ values will further decrease; a similar trend also appears in the $D_s$ values with flame, as shown in Fig. 6b, and hence, the presence of ZB and $Sb_2O_3$ can effectively suppress the smoke production during the burning of the sample. On the other hand, it clearly shows a significant decrease in $D_s$ values with the addition of ZB and $Sb_2O_3$ under a radiant heat flux of 50 kW $m^{-2}$ without flame from Fig. 7a; however, the IFR-1 coating containing only EG shows an ineffective smoke suppression. It can be illustrated that the EG char is not nearly so strong as the

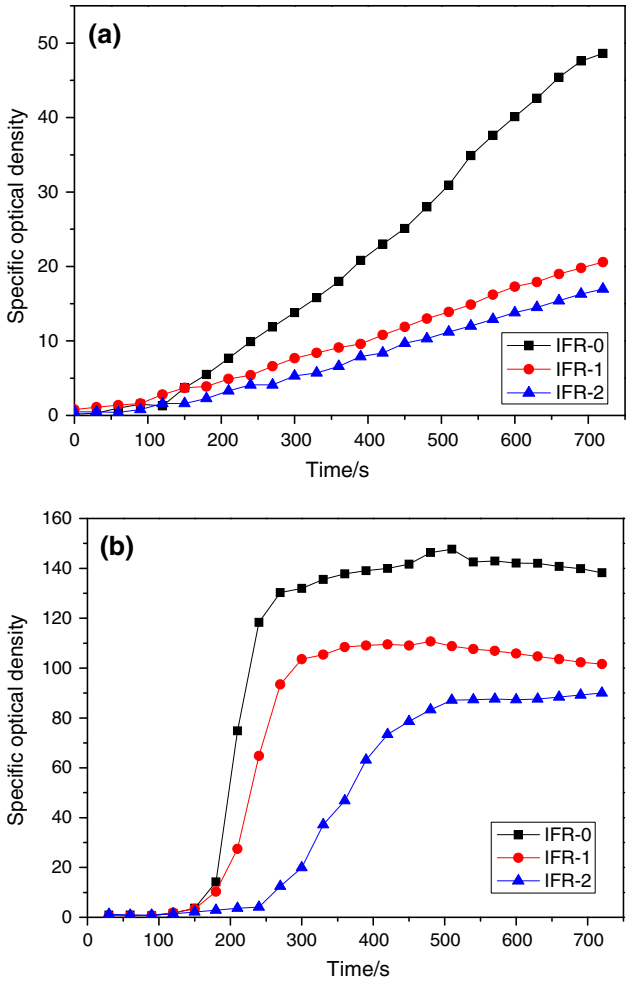


**Fig. 6** Specific optical density curves of the epoxy-based IFR coatings without (**a**) and with (**b**) flame at a flux of 25 kW $m^{-2}$

residual char of the IFR-2 coating to retard the continuous heat and smoke under high heat flux.

Note that the $D_s$ values of the IFR-2 coating are just slightly lower than those of other samples under a radiant heat flux of 50 kW $m^{-2}$ with flame, as shown in Fig. 7b. It implies that the ZB and $Sb_2O_3$ can effectively suppress the smoke through molten protective layer on the surface of the samples, during the combustion process; however, there is no effective synergistic smoke suppression in the gas phase, so that the combustible materials derived from the degradation will be ignited to generate smoke continuously. These results reveal that the excellent synergistic smoke suppression effect of ZB and $Sb_2O_3$ is mainly in the condensed phase.

## Scanning electron microscopy of char residue

The residual char of the IFR coatings, which acts as a barrier to prevent the burning of combustible materials

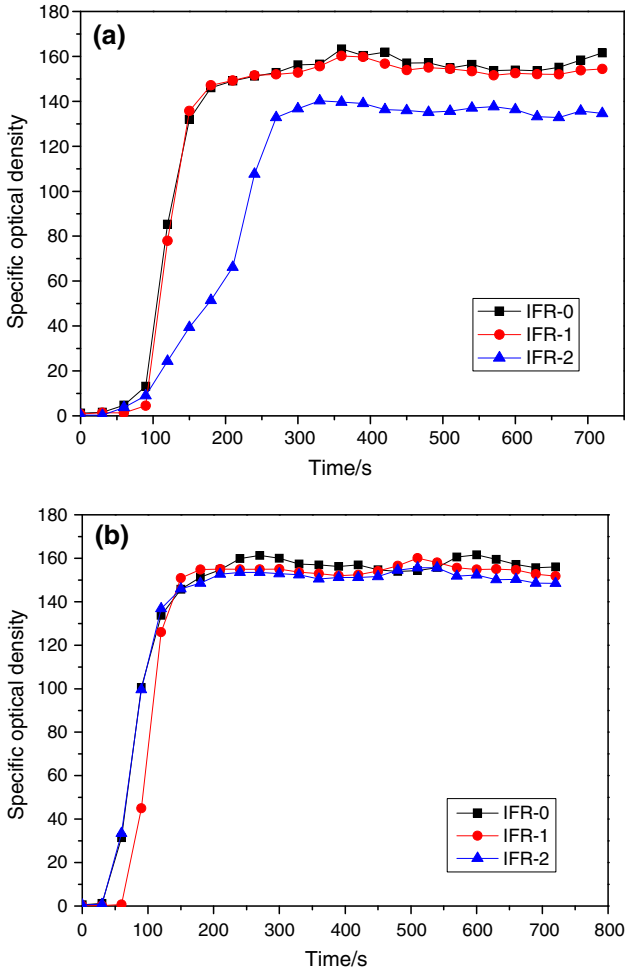


**Fig. 7** Specific optical density curves of the epoxy-based IFR coatings without (**a**) and with (**b**) flame at a flux of 50 kW $m^{-2}$

decomposed from the underlying materials, the heat transfer and the entrance of oxygen, plays an important role in the flame retardancy performance and smoke suppression. In order to investigate the impact of the residual char on the flame retardancy and smoke suppression, the structures of the chars for different IFR coating systems were characterized. Figure 8 shows the digital photographs (labeled by IFR-0, IFR-1 and IFR-2) and scanning electron microscopy (SEM) micrographs (labeled by IFR-0S, IFR-1S and IFR-2S) of the residual chars for the epoxy-based IFR coatings after cone calorimeter test.

From the digital photographs, it can be seen that the residual char of the IFR-0 is the thinnest and loosest so that it will easily fall off and the shape of the char is difficult to retain. The swollen char of the IFR-1 tends to be more connective and compact, and thus can provide a protective layer to retard the flaming, as a result. However, there are many obvious gaps around the expanded graphite char. Note that the IFR-2 shows the densest and smoothest residual char surface among all samples, responding to the lowest HRR, THR and a series of data tested by cone calorimeter.

On the other hand, the residual chars of the three coatings show different structures as well, according to the SEM micrographs. Specifically, the residual char of the IFR-0S is very thin and porous, while that of the IFR-1S is thick and worm-like. However, there are some obviously large holes and crevices on the char surface of the IFR-1S, and it has a negative impact on the flame retardancy and smoke suppression. Another point worthy to be discussed is that the residual char of the IFR-2S is smooth and compact, which provides a good shielding effect in combustion; furthermore, the residual chars are tightly associated with the glassy layer derived from the molten ZB, and the good interfacial adhesion between them can accelerate the formation of a denser char layer.

## Thermogravimetric analysis/Fourier transform infrared spectrometry

The synergistic effect of ZB and $Sb_2O_3$ on flame retardancy and smoke suppression will be further investigated by the data from the TG analyses. Figure 9 gives the TG and DTG curves of the IFR-1 and IFR-2 coatings in nitrogen atmosphere, and the corresponding characteristic parameters, such as the initial decomposition temperature ($T_d$) considered as the temperature at which the mass loss of the sample reaches 5 mass%, the temperature at the maximum degradation rate ($T_{max}$) and char yield ($Y_c$) at 700 °C, are summarized in Table 2.

It can be seen that the IFR-2 coating has a greatly higher $T_d$ value than that of the IFR-1 coating; however, unexpectedly, the $T_{max1}$ value of the IFR-2 coating is lower than that of the IFR-1 coating. This phenomenon can be attributed to the reaction between the $Sb_2O_3$ and phosphate, so that the APP will decompose to form phosphate more quickly at a low temperature, as discussed above.

In addition, both ZB and $Sb_2O_3$ tend to absorb a massive source of heat during the melting process, and hence, the decomposition reaction will slow down accordingly. Moreover, the molten protective layer derived from the ZB and $Sb_2O_3$ can effectively enhance the thermal stability of the sample, and thus, both the $T_{max2}$ and $T_{max3}$ values of the IFR-2 coating are higher than that of the IFR-1 coating. This will be further confirmed by the $Y_c$ values.

The IFR-2 coating has a much higher $Y_c$ value than the IFR-1 coating; hence, the incorporation of ZB and $Sb_2O_3$ can promote the formation of more stable residues at high temperature. This is one factor leading to the excellent synergistic flame retarding and smoke suppression effect of ZB and $Sb_2O_3$.

The thermogravimetric analysis and Fourier transform infrared spectrometry (TG-FTIR) spectra further disclose

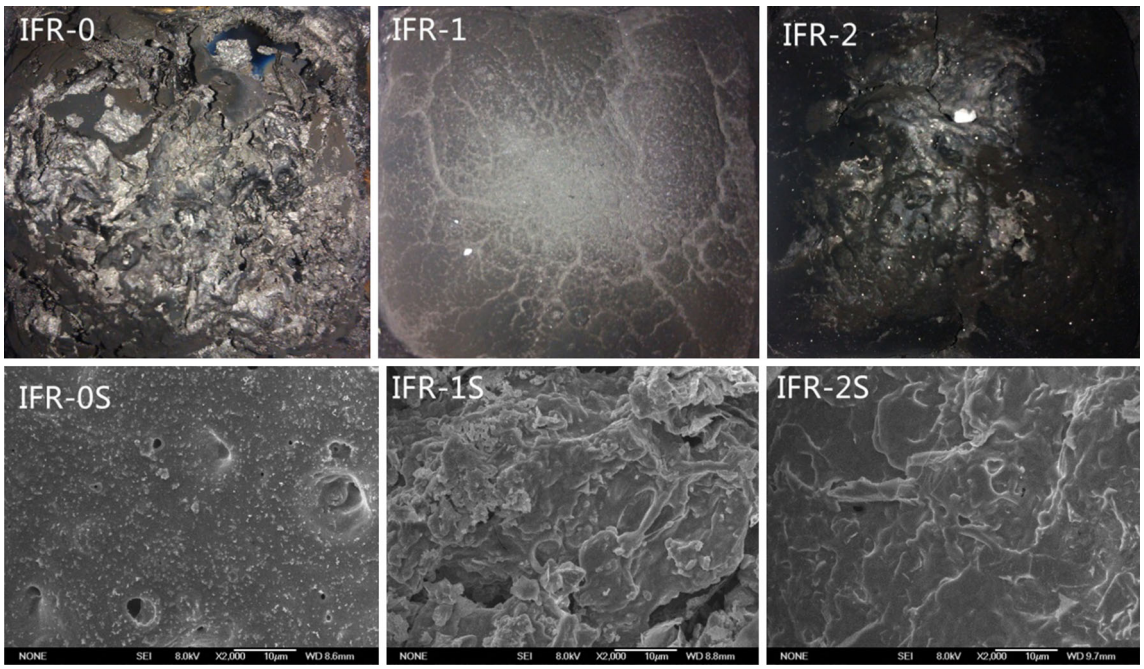


**Fig. 8** Digital photographs and SEM micrographs of char residue of the epoxy-based IFR coatings

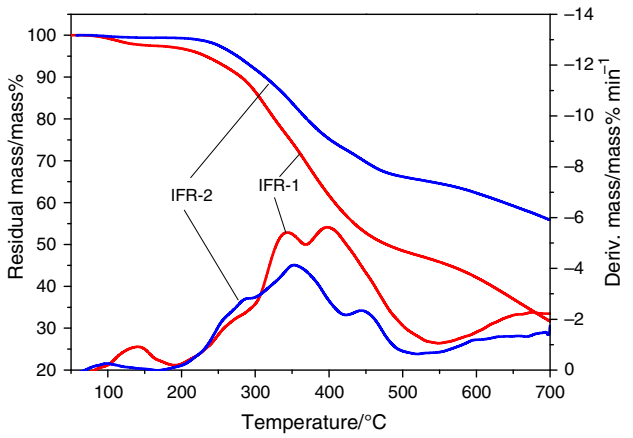


**Fig. 9** TG and DTG curves of the IFR-1 and IFR-2 coatings at a constant heating rate of 20 K min$^{-1}$

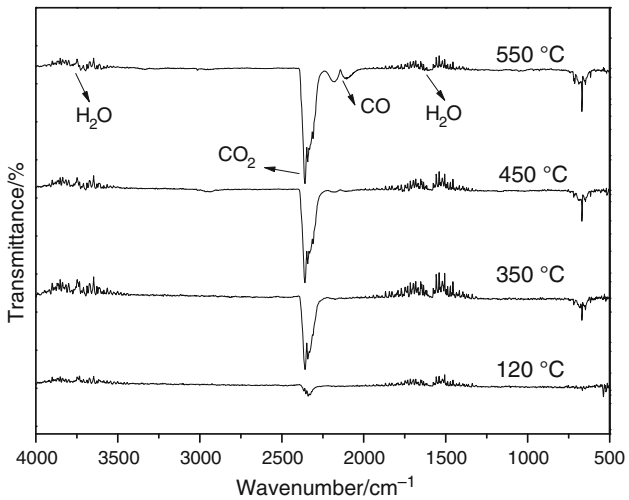


**Fig. 10** FTIR spectra of pyrolysis gas products of the IFR-1 coating at different temperatures

**Table 2** Characteristic data from TG analyses in a $N_2$ atmosphere at heating rate of 20 K min$^{-1}$

| Sample | $T_d$/°C | $T_{max1}$/°C | $T_{max2}$/°C | $T_{max3}$/°C | $Y_c$/mass% |
|---|---|---|---|---|---|
| IFR-1 | 232.8 | 114.2 | 316.4 | 370.6 | 31.6 |
| IFR-2 | 275.7 | 98.3 | 352.7 | 440.9 | 55.9 |

the pyrolysis information so that the main compositions of the gas products from the thermal degradation process can be inferred. Figures 10 and 11 show the TG-FTIR spectra of the IFR-1 and IFR-2 coatings at the heating rate of 20 K min$^{-1}$. It can be seen that the wavenumber range of 3100–2600 cm$^{-1}$ is assigned to the absorption peak for carbon dioxide, the wavenumber range of 4000–3400 and 2060–1260 cm$^{-1}$ is assigned to the absorption peak for water vapor, and the wavenumber range of 2260–1990 cm$^{-1}$ is assigned to the absorption peak for carbon monoxide.

In the spectrum of the IFR-2 coating, there are some obvious absorption peaks for $H_2O$ and $CO_2$ at 120 °C; however, for the IFR-1 coating, the absorption peaks for

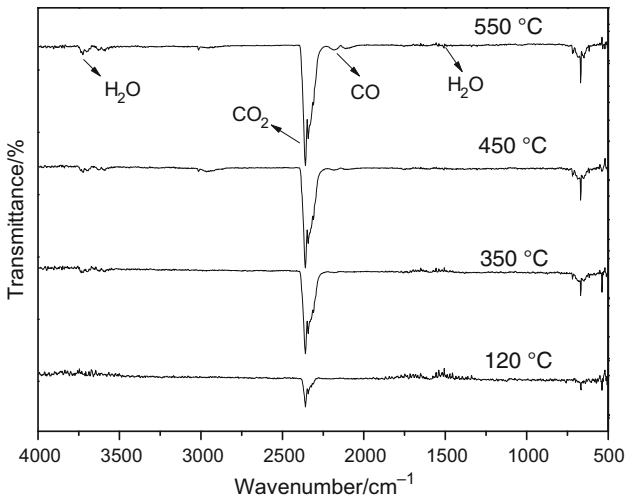


**Fig. 11** FTIR spectra of pyrolysis gas products of the IFR-2 coating at different temperatures

$CO_2$ are a little weaker, indicating that the initial decomposition of the IFR-2 coating is earlier than that of the IFR-1 coating. In addition, the absorption peaks for $H_2O$ of the IFR-2 coating at 350 and 450 °C are not obvious, but the absorption peaks for $H_2O$ of the IFR-1 coating are quite strong. These results suggest that a lot of heat tends to be absorbed in the process of the melting of ZB and $Sb_2O_3$, which slows the thermal degradation process down. Thus, the water vapor derived from the degradation will be barely detected. The absorption peaks for CO visibly appear in the spectrum of the IFR-1 coating at 550 °C, while the absorption peaks for CO are weak for the IFR-2 coating, suggesting that the IFR-2 coating has a lower CO yield, which can hence be attributed to the good shielding effect of the residual char of the IFR-2 coating.

## Conclusions

With the addition of ZB and $Sb_2O_3$, the epoxy-based IFR coating can effectively suppress smoke and retard heat during the whole combustion process. The ZB and $Sb_2O_3$ can improve the shielding layer to be more stable and compact, so that it can restrain the smoke generation and heat release. Moreover, a lot of heat will be absorbed during the melting process of ZB and $Sb_2O_3$. In summary, the smoke suppression and synergistic flame retardancy properties of ZB and $Sb_2O_3$ in epoxy-based IFR coating are quite excellent.

**Acknowledgements** The authors gratefully acknowledge the financial support from the National Natural Science Foundation of China (NSFC No. 51006054), Shandong Provincial Natural Science Foundation of China (ZR2014EEM037), the Key Laboratory of Fire Prevention and Rescue Technology (KF201405) and State Key Laboratory of Safety and Control for Chemicals of China (SKL-023).

## References

1. Lai X, Zeng X, Li H, Zhang H. Effect of polyborosiloxane on the flame retardancy and thermal degradation of intumescent flame retardant polypropylene. J Macromol Sci B. 2014;53:721–34.
2. Chen X, Sun T, Cai X. The investigation of intumescent flame-retarded ABS using zinc borate as synergist. J Therm Anal Calorim. 2013;115:185–91.
3. Zhang C, Zhang F. Removal of brominated flame retardant from electrical and electronic waste plastic by solvothermal technique. J Hazard Mater. 2012;221:193–8.
4. Zhou K, Zhang Q, Liu J, Wang B, Jang S, Shi Y, Hu Y, Gui Z. Synergetic effect of ferrocene and $MoS_2$ in polystyrene composites with enhanced thermal stability, flame retardant and smoke suppression properties. RSC Adv. 2014;4:13205–14.
5. Li J, Ke C, Xu L, Wang Y. Synergistic effect between a hyperbranched charring agent and ammonium polyphosphate on the intumescent flame retardance of acrylonitrile–butadiene–styrene polymer. Polym Degrad Stab. 2012;97:1107–13.
6. Almeras X, Bras ML, Hornsby P, Bourbigot S, Marosi G, Keszeid S, Poutche F. Effect of fillers on the fire retardancy of intumescent polypropylene compounds. Polym Degrad Stab. 2003;82:325–31.
7. Liu Q, Bao X, Deng SQ, Cai XF. The investigation of methyl phenyl silicone resin/epoxy resin using epoxy–polysiloxane as compatibilizer. J Therm Anal Calorim. 2014;118:247–54.
8. Lu H, Song L, Hu Y. A review on flame retardant technology in China. Part II: flame retardant polymeric nanocomposites and coatings. Polym Adv Technol. 2011;22:379–94.
9. Zhang F, Wang Y, Li SX, Zhang J. Influence of thermophysical properties on burning behaviour of intumescent fire-retardant materials. J Therm Anal Calorim. 2013;113:803–10.
10. Chen X, Jiao C, Zhang J. Microencapsulation of ammonium polyphosphate with hydroxyl silicone oil and its flame retardance in thermoplastic polyurethane. J Therm Anal Calorim. 2011;104:1037–43.
11. Chen X, Jiao C, Li S, Sun J. Flame retardant epoxy resins from bisphenol-A epoxy cured with hyperbranched polyphosphate ester. J Polym Res. 2011;18:2229–37.
12. Levchik S, Piotrowski A, Weil E, Yao Q. New developments in flame retardancy of epoxy resins. Polym Degrad Stabil. 2005;88:57–62.
13. Zhu P, Chen Y, Wang LY, Qian GY, Zhou M, Zhou J. A new technology for separation and recovery of materials from waste printed circuit boards by dissolving bromine epoxy resins using ionic liquid. J Hazard Mater. 2012;239–240:270–8.
14. Bučko M, Mišković-Stanković V, Rogan J, Bajat JB. The protective properties of epoxy coating electrodeposited on Zn–Mn alloy substrate. Prog Org Coat. 2015;79:8–16.
15. Chen X, Jiang Y, Jiao C. Smoke suppression properties of ferrite yellow on flame retardant thermoplastic polyurethane based on ammonium polyphosphate. J Hazard Mater. 2014;266:114–21.
16. Zhou K, Yang W, Tang G, Wang BB, Jiang SH, Hu Y, Gui Z. Comparative study on the thermal stability, flame retardancy and smoke suppression properties of polystyrene composites containing molybdenum disulfide and graphene. RSC Adv. 2013;3:25030–40.
17. Chen J, Liu S, Jiang Z, Zhao JQ. Flame retardancy, smoke suppression effect and mechanism of aryl phosphates in combination with magnesium hydroxide in polyamide 6. J Wuhan Univ Technol. 2012;27:916–23.
18. Levchik SV, Weil ED. Thermal decomposition, combustion and flame-retardancy of epoxy resins? A review of the recent literature. Polym Int. 2004;53:1901–29.

19. Ge L, Duan H, Zhang X, Chen C, Tang JH, Li ZM. Synergistic effect of ammonium polyphosphate and expandable graphite on flame-retardant properties of acrylonitrile–butadiene–styrene. J Appl Polym Sci. 2012;126:1337–43.
20. Doğan M, Bayramlı E. The flame retardant effect of aluminum phosphinate in combination with zinc borate, borophosphate, and nanoclay in polyamide-6. Fire Mater. 2014;38:92–9.
21. Lu H, Wilkie CA. Synergistic effect of carbon nanotubes and decabromodiphenyl oxide/$Sb_2O_3$ in improving the flame retardancy of polystyrene. Polym Degrad Stab. 2010;95:564–71.
22. Jiao C, Chen X. Flammability and thermal degradation of intumescent flame-retardant polypropylene composites. Polym Eng Sci. 2010;50:767–72.
23. Fang S, Hu Y, Song L, He QL. Mechanical properties, fire performance and thermal stability of magnesium hydroxide sulfate hydrate whiskers flame retardant silicone rubber. J Mater Sci. 2007;43:1057–62.
24. Han J, Liang G, Gu A, Ye JH, Zhang ZY, Yuan L. A novel inorganic–organic hybridized intumescent flame retardant and its super flame retarding cyanate ester resins. J Mater Chem. 2013;A1:2169–82.
25. Li N, Xia Y, Mao Z, Guan Y, Zheng AN. Influence of antimony oxide on flammability of polypropylene/intumescent flame retardant system. Polym Degrad Stab. 2012;97:1737–44.
26. Ricciardi MR, Antonucci V, Zarrelli M, Giordano M. Fire behavior and smoke emission of phosphate-based inorganic fire-retarded polyester resin. Fire Mater. 2012;36:203–15.
27. Cogen JM, Lin TS, Lyon RE. Correlations between pyrolysis combustion flow calorimetry and conventional flammability tests with halogen-free flame retardant polyolefin compounds. Fire Mater. 2009;33:33–50.
28. Wang D, Zhang Q, Zhou K, Yang W, Hu Y, Gong XL. The influence of manganese–cobalt oxide/graphene on reducing fire hazards of poly(butylene terephthalate). J Hazard Mater. 2014;278:391–400.